



## Voxel-based analysis of diffusion tensor imaging in patients with mesial temporal lobe epilepsy



Patrícia Sanches <sup>a,b</sup>, Elaine Keiko Fujisao <sup>a</sup>, Aline M.S. Braga <sup>a</sup>, Nathalia Raquel Cristaldo <sup>a</sup>, Roberto dos Reis <sup>a,b</sup>, Seizo Yamashita <sup>b</sup>, Luiz Eduardo Betting <sup>a,\*</sup>

<sup>a</sup> Departamento de Neurologia, Psicologia e Psiquiatria, Faculdade de Medicina de Botucatu – UNESP – Univ Estadual Paulista, Brazil

<sup>b</sup> Departamento de Doenças Tropicais e Diagnóstico por Imagem, Faculdade de Medicina de Botucatu – UNESP – Univ Estadual Paulista, Brazil

### ARTICLE INFO

#### Article history:

Received 14 May 2016

Received in revised form 19 February 2017

Accepted 24 March 2017

Available online 25 March 2017

#### Keywords:

Temporal lobe epilepsy

Hippocampal sclerosis

Neuroimaging

Diffusion tensor imaging

### ABSTRACT

**Purpose:** Quantitative techniques of diffusion analysis allow for an in-vivo investigation of the physiopathology of epilepsies. The objective of this study was to evaluate the variation of the main diffusion parameters and explore differences between two methodologies of voxel-wise analysis comparing a group of patients with mesial temporal lobe epilepsy (MTLE) with controls.

**Methods:** 24 patients with a diagnosis of MTLE were selected. All patients and a control group of 36 individuals were submitted to 3T magnetic resonance imaging. Diffusion parameters were obtained from the raw images. Based on the tensors, a customized template was created, and images were registered into standard space. Voxel-based comparisons between patients and controls was performed by whole brain voxel-wise analysis and tract-based spatial statistics (TBSS). Tract-specific analysis (TSA) was performed in the mostly damaged fasciculi.

**Results:** 10 patients presented with right hippocampal sclerosis (HS), 11 with left HS and 3 with bilateral HS with left predominance. Whole brain voxel-wise analysis showed abnormalities mainly localized in the temporal lobes (total volume of 3859 mm<sup>3</sup>). TBSS showed more widespread abnormalities (21931 mm<sup>3</sup>). TSA pointed to abnormalities situated essentially in the temporal stem topography. Fractional anisotropy (FA) and radial diffusivity (RD) were the parameters that showed more abnormalities.

**Conclusion:** Whole brain voxel-wise analysis was more restricted than TBSS. The methods were complementary stressing the significance of the findings. The abnormalities were more frequently observed in FA and RD indicating the need for using several diffusion parameters for the investigation of patients with MTLE.

© 2017 Elsevier B.V. All rights reserved.

## 1. Introduction

Investigations of the white matter in patients with mesial temporal lobe epilepsy (MTLE) using diffusion tensor imaging (DTI) have been able to detect abnormalities predominantly, but unrestricted to, the temporal lobe allocated in a centrifugal pattern (Concha et al., 2012). This pattern is under investigation and changes according to the heterogeneity of the patients and the different methods of neuroimaging analysis, including the acquisition parameters and post-processing algorithms.

Voxel-based analyses are quantitative techniques which have as major advantages the ability to statistically compare groups of brains (Yasuda et al., 2010). In diffusion images, voxel-based anal-

yses may be performed directly in the diffusion maps using an analogous methodology of the voxel-based morphometry (VBM) (Ashburner and Friston, 2000). The main drawback with this approach comes from incorrect registration of the images which, is considered a critical problem in DTI (Bookstein, 2001; Abe et al., 2010).

Another widely used technique is tract-based spatial statistics (TBSS) (Smith et al., 2006). This methodology consists in projecting the diffusion data onto a simplified map of the white-matter. The main objective of TBSS creation was to overcome the registration problem. However, limitations, especially concerning this issue and the direction of the tracts, still exist (Bach et al., 2014; Schwarz et al., 2014).

Improved voxel-based analyses of diffusion images may be achieved using tensor-based registration (Keihaninejad et al., 2013). Because whole brain voxel-wise analysis and TBSS are performed with different approaches, the main hypothesis is that they may show different aspects of the abnormalities in patients with

\* Corresponding author at: Departamento de Neurologia, Psicologia e Psiquiatria, Faculdade de Medicina de Botucatu – UNESP – Univ Estadual Paulista, Zip Code 18618-687, Botucatu, SP, Brazil.

E-mail address: [betting@fmb.unesp.br](mailto:betting@fmb.unesp.br) (L.E. Betting).

MTLE. In addition, differences may also be observed depending on the diffusion parameter used. The objective of this investigation was a multimodal investigation of tensor-based registered DTI images of patients with MTLE.

## 2. Methods

This study was approved by the local ethics committee. Patients with refractory MTLE ( $n=24$ , 16 women, mean age  $42 \pm 12$  years, range 20–68) and with hippocampal sclerosis (HS) were selected. Diagnosis of MTLE was performed according to clinical and electroencephalographic features following previous recommendations (Commission on Classification and Terminology of the International League Against Epilepsy, 1989; Berg et al., 2010). All patients had focal seizures which were detailed by clinical history obtained from patients or relatives. Patients with dual pathology or extra-temporal epilepsy were excluded. Control subjects ( $n=36$ , 18 women, mean age  $33 \pm 11$  years, range 21–57) without histories of neurologic disease were recruited from the local community. All subjects gave informed consent.

### 2.1. Electroencephalogram (EEG)

Interictal EEG was performed with a 32-channel recorder (Nihon Kohden, Tokyo, Japan). Electrodes were positioned according to the 10–20 international system of electrode placement and with additional Silverman's anterior temporal electrodes. All records were performed with 20 min long, with photic stimulation and hyper-ventilation.

### 2.2. Magnetic resonance imaging (MRI)

MRI acquisitions were performed using a 3 T scanner (Siemens, Verio, Erlangen, Germany) with a 12-channel head array coil.

HS was diagnosed by conventional visual examination based on two main sequences: coronal perpendicular to the long axis of the hippocampus defined at the sagittal image Short T1 inversion recovery (STIR; slice thickness, 2.2 mm; field-of-view (FOV), 180 mm; matrix size,  $230 \times 256$ ; repetition time (TR), 2100 ms; echo time (TE), 9.5 ms; inversion time (TI), 499 ms; flip angle, 150°; acquisition time, 3.36 min) and T2 periodically rotated overlapping parallel lines with enhanced reconstruction (BLADE; slice thickness, 2.2 mm; FOV, 180 mm; matrix size,  $230 \times 256$ ; TR, 4000 ms; TE, 135 ms; flip angle, 120°; acquisition time, 3.22 min).

For hippocampal and whole brain volumetry, three-dimensional Magnetization Prepared Rapid Gradient Echo T1 sequences (MPRAGE; 192 sagittal slices; slice thickness, 1 mm; in plane resolution,  $0.5 \times 0.5$  mm; FOV, 256 mm; matrix size,  $256 \times 256$ ; TR, 2300 ms; TE, 2.47 ms; TI, 1100 ms; flip angle, 9°; acquisition time, 5.21 min per volume) were used.

Diffusion weighted images were acquired using single-shot echo planar imaging (65 axial slices; slice thickness, 2 mm; in plane resolution,  $1.8 \times 1.8$  mm; 12 non collinear diffusion gradients direction, b-value  $1000 \text{ s/mm}^2$ ; FOV, 230 mm; matrix size  $128 \times 128$  mm; TR, 9100 ms; TE, 96 ms; TI, 200 ms; flip angle, 150°; 4 averages to improve signal-to-noise ratio; total acquisition time, 8.21 min). Images were acquired in Digital Imaging and Communications in Medicine (DICOM) format and transformed into ANALYZE and the Neuroimaging Informatics Technology Initiative (NIfTI) format using MRIcron software (Rorden and Brett, 2000).

### 2.3. Hippocampal volumetry

The FreeSurfer (<http://surfer.nmr.mgh.harvard.edu/>), version 5.3, developed at the Martinos Center for Biomedical Imaging by the Laboratory for Computational Neuroimaging, Charlestown,

MA, U.S.A.) image analysis suite was used to obtain hippocampal volumes and total intracranial volumes (TIV). Volumetry was performed to confirm HS and to group the patients according to the most atrophic hippocampus for bilateral HS. The standard processing pipeline implemented in the software was used. ANALYZE images were imported into the software, and they automatically underwent several processing steps including motion correction, non-brain tissue removal, automatic registration into Talairach space, segmentation of subcortical structures including the hippocampus, and tessellation of gray matter white matter boundaries (Fischl et al., 2002; Fischl et al., 2004).

Hippocampal volumes were normalized according to the TIV. An asymmetry index was calculated by:  $2 \times (\text{right hippocampus} - \text{left hippocampus}) \div (\text{right hippocampus} + \text{left hippocampus})$ . The volumes and the asymmetry index obtained for each individual were standardized according to the value of normal controls using a z-score transformation.

### 2.4. Diffusion tensor imaging processing

FSL software (FMRIB Software Library, [www.fmrib.ox.ac.uk/fsl](http://www.fmrib.ox.ac.uk/fsl), version 5.0, created by the Analysis Group, FMRIB, Oxford, U.K.) was used to obtain the main diffusion maps (Jenkinson et al., 2012). NIfTI images were imported and submitted to brain extraction followed by eddy currents correction using the Brain Extraction Tool (BET) and FMRIB's Diffusion Toolbox (FDT) (Smith, 2002; Behrens et al., 2003). Finally, a diffusion tensor model was fitted at each voxel using DTIFIT (Behrens et al., 2003). After these steps, the DTI parameters obtained were imported into DTI-TK software ([www.nitrc.org/projects/dtitk](http://www.nitrc.org/projects/dtitk), developed at Penn Image Computing and Science Laboratory, University of Pennsylvania, Philadelphia, PA, U.S.A.) for further processing. This software provides an algorithm to register DTI images aligning white matter tracts by combining the fiber orientation in each voxel (Keihaninejad et al., 2013; Wang et al., 2011).

Using DTI-TK, a customized template was created. All images were submitted to an initial rigid alignment with a template based on 550 normal individuals with ages between 20 and 80 years (Zhang et al., 2010). To obtain the customized template, images were subsequently submitted to affine linear alignment and to a diffeomorphic registration algorithm with 6 iterations. After the creation of this specific template, it was individually submitted to rigid, affine and diffeomorphic alignment with a specific enhanced DTI template in ICBM-152 space (International Consortium for Brain Mapping, Montreal Neurological Institute, MNI) (Zhang et al., 2011). Finally, deformation fields obtained for the creation and ICBM-152 transformation of the template were applied for each individual in the study. The final results were aligned images in the standard space with 1 mm isotropic voxels. For each subject, diffusion parameter maps of fractional anisotropy (FA), axial diffusivity (AD), radial diffusivity (RD) and mean diffusivity (MD) were finally extracted and used for statistical analysis.

### 2.5. Statistical analysis

Two types of voxel-based comparisons were conducted. A whole brain voxel-based analysis was performed using SPM12 ([www.fil.ion.ucl.ac.uk/spm](http://www.fil.ion.ucl.ac.uk/spm), Wellcome Trust Centre for Neuroimaging, University College London, London, U.K.) running under the Matlab R2012b platform (MathWorks, Natick, MA, U.S.A.). In this method, diffusion images were smoothed with an 8 mm Gaussian filter (Full Width at Half Maximum). For each diffusion parameter, comparisons between patients and controls were performed using a full factorial design with two contrasts (searching for areas of increased and decreased abnormalities).

**Table 1**

Clinical, electroencephalographic and neuroimaging features of 24 patients with mesial temporal lobe epilepsy.

N	HS	First	Freq	Medications	EEG	Age	Gender	RH vol	RH z	LH vol	LH z	AI z
1	L	8	0	CBZ 1200, LTG 100, CLB 60	Normal	52	Women	3766	0.8	2422	-4.3	9.1
2	L	25	3	LTG 300, CLB 20	Left	58	Men	3894	-0.3	2866	-3.8	6.2
3	R	1	2	TPM 300, PHT 300	Right, Slow	43	Women	2911	-3.2	4213	1.6	-8.6
4	R	11	2	OXC 2100, VPA 1000, CLB 20	Bilateral	33	Men	2809	-4.1	3700	-1.1	-6.5
5	L	12	2	LTG 450, CLB 40	Left	28	Women	3919	-0.4	2532	-5.2	9.0
6	L	10	4	CLB 20, PB 50, CBZ 1000	Left	37	Women	4469	1.4	3907	-0.1	2.5
7	L	7	3	CBZ 1000	Slow	22	Women	4122	1.2	2805	-3.5	7.9
8	L	3	3	PHT 300, CLB 10	Left	58	Men	4153	3.0	2749	-2.4	8.5
9	B	2	0	CBZ 1200, CLB 10	Right	49	Women	2489	-4.4	2411	-5.0	0.2
10	R	17	8	CBZ 600, CLB 20	Right	26	Men	3846	-2.6	4248	-1.4	-2.7
11	R	10	4	CBZ 1200	Right	39	Women	3814	-2.0	4633	0.8	-4.8
12	R	13	6	CBZ 600, LTG 400	Right	61	Women	3629	-1.3	4600	2.5	-5.7
13	R	28	20	CBZ 1200, CLB 20	Right	42	Women	4133	-0.8	4405	0.3	-2.0
14	L	10	4	CBZ 1200, CLB 40	Left	39	Women	4392	0.7	2884	-4.2	8.6
15	L	10	2	PB 100, CBZ 400	Left	41	Men	4304	0.9	3349	-2.2	5.0
16	R	12	20	CBZ 400, CLB 40, TPM 400	Right	37	Women	3110	-3.9	3967	-1.2	-5.8
17	L	5	12	CBZ 1200, CLB 20	Left	37	Women	3353	-1.0	2372	-4.9	7.1
18	R	21	10	CBZ 200, CLB 60	Bilateral	40	Women	3017	-3.5	4494	1.7	-9.2
19	B	7	1	TPM 125, CLB 10	Bilateral	60	Women	2918	-3.9	2205	-6.7	5.6
20	B	5	4	CBZ 1200	Left	43	Women	2442	-4.9	2231	-6.1	1.5
21	L	2	2	CBZ 600, PHT 200, PB 100	-	43	Men	3899	-0.6	2503	-5.4	9.1
22	R	42	8	CBZ 1000	Bilateral	58	Women	3420	-1.2	3852	0.6	-3.1
23	L	7	-	CBZ 1000	Left	68	Men	3818	-1.5	2835	-4.7	6.0
24	R	4	3	CBZ 1200, CLB 20	Normal	20	Men	2577	-5.2	3888	-1.1	-9.4

N, Number of patients; HS, hippocampal sclerosis (R, right; L, left; B, bilateral); First, age at first seizure in years; Freq, estimated number of seizures per month; medications, daily doses in mg of the antiepileptic medications in use at the time of magnetic resonance acquisition (CBZ, carbamazepine, LTG, lamotrigine; CLB, clobazam; TPM, topiramate; PHT, phenytoin; OXC, oxcarbazepine; VPA, valproate; PB, phenobarbital); EEG, result of the record with indication of epileptiform discharge lateralization; slow, slow background; Age reported in years; RH vol, volume of the right hippocampus (raw, not normalized) in mm<sup>3</sup>; RH z/LH z, z-score of the right/left hippocampus after normalization; LH vol, volume of the left hippocampus (raw, not normalized) in mm<sup>3</sup>; AI z, z-score of the asymmetry index after normalization.

The second type of voxel-based analysis used was TBSS. Based on the FA images, a mean skeleton of the white matter of the whole group was created. For each parameter, the values of white matter tracts of all individuals were projected in this FA skeleton. Comparisons between each parameter of patients and controls were performed using Randomise, an FSL tool for nonparametric permutation inference (Winkler et al., 2014). Two contrasts searching for areas of increased and decreased abnormalities and 5000 permutations were used.

After the statistical analysis, a Talairach atlas was used to identify the nearest gray matter anatomical structure (Talairach and Tournoux, 1988). For the identification of the main fasciculi involved, the Johns Hopkins University (JHU) white-matter tractography atlas was used (Mori, 2005). This probabilistic atlas identified 20 main structures in 28 individuals (Mori, 2005).

Finally, to confirm the results a tract-specific analysis (TSA) was performed for the main tracts depicted in the previous steps. Using DTI-TK, samples of the white matter and tract-specific attributes across the whole population were obtained. The mean value was projected onto a medial two dimensional model representing the real tridimensional tracts. For each individual the values corresponding to the spokes from each vertex of the mesh were obtained and used for the analysis (Yushkevich et al., 2008). Statistical analysis was performed comparing the tracts of patients and controls using a general linear model with two contrasts (increased and decreased differences).

For the three types of analyses, age, sex and TIV were introduced as covariates. The level of significance selected was  $p < 0.05$  corrected for multiple comparisons (Family-Wise Error and for TBSS with additional Threshold-Free Cluster Enhancement).

### 3. Results

#### 3.1. Clinical and EEG findings

The mean age of recurrent seizures onset was  $10 \pm 9$  years (range, 1–42). At the time of MRI acquisition, the mean fre-

quency of focal seizures estimated according to clinical history was  $5 \pm 5$  per month (0–20) and the patients were using a mean of  $2 \pm 1$  antiepileptic drugs (1–3). Interictal EEG showed epileptiform discharges in the left anterior temporal region in 9 patients. Meanwhile, 7 patients showed discharges in the right anterior temporal region, and 4 had bilateral discharges. Two patients presented with normal EEGs, 1 patient had abnormal background activity and 1 patient was not subjected to the exam. The clinical and EEG findings are reported in Table 1.

#### 3.2. MRI findings

Hippocampal volumetry confirmed that 10 patients presented with left HS, 11 with right HS, and 3 with bilateral HS with left predominance. The mean volume of the left hippocampus was  $4315 \pm 363$  (3428–4961) for the controls and  $3336 \pm 848$  (2205–4633) mm<sup>3</sup> for the patients. The mean volume of the right hippocampus was  $4412 \pm 362$  (3682–5268) for the controls and  $3550 \pm 626$  (2442–4469) mm<sup>3</sup> for the patients. After normalization, the z-scores obtained for the patients were  $-2.1 \pm 2.7$  ( $-6.7$ – $2.8$ ) for the left and  $-1.4 \pm 2.2$  ( $-5.2$ – $3$ ) for the right hippocampus. The mean asymmetry index was  $1.1 \pm 5.6$  ( $-9.4$ – $9.1$ ). These findings are detailed in Table 1 and Fig. 1.

#### 3.3. Whole brain voxel-wise analysis

For the whole group of patients, we obtained: one cluster of increased AD, volume of 290 mm<sup>3</sup>, main localization in the right parahippocampal gyrus ( $x = 31$ ,  $y = -18$ ,  $z = -24$ ; T value = 6.11; Z = 5.32; p = 0.001); two clusters of increased RD, total volume of 1102 mm<sup>3</sup>, main localization in the right parahippocampal gyrus ( $x = 28$ ,  $y = -16$ ,  $z = -25$ ; T value = 6.65; Z = 5.67; p < 0.0001); two clusters of increased MD, total volume of 782 mm<sup>3</sup>, main localization in the right parahippocampal gyrus ( $x = 29$ ,  $y = -17$ ,  $z = -24$ ; T value = 6.52; Z = 5.59; p < 0.0001); five clusters of reduced FA, total volume of 1685 mm<sup>3</sup>, main localization in the left temporal lobe involving the uncinate and inferior fronto-occipital fasci-

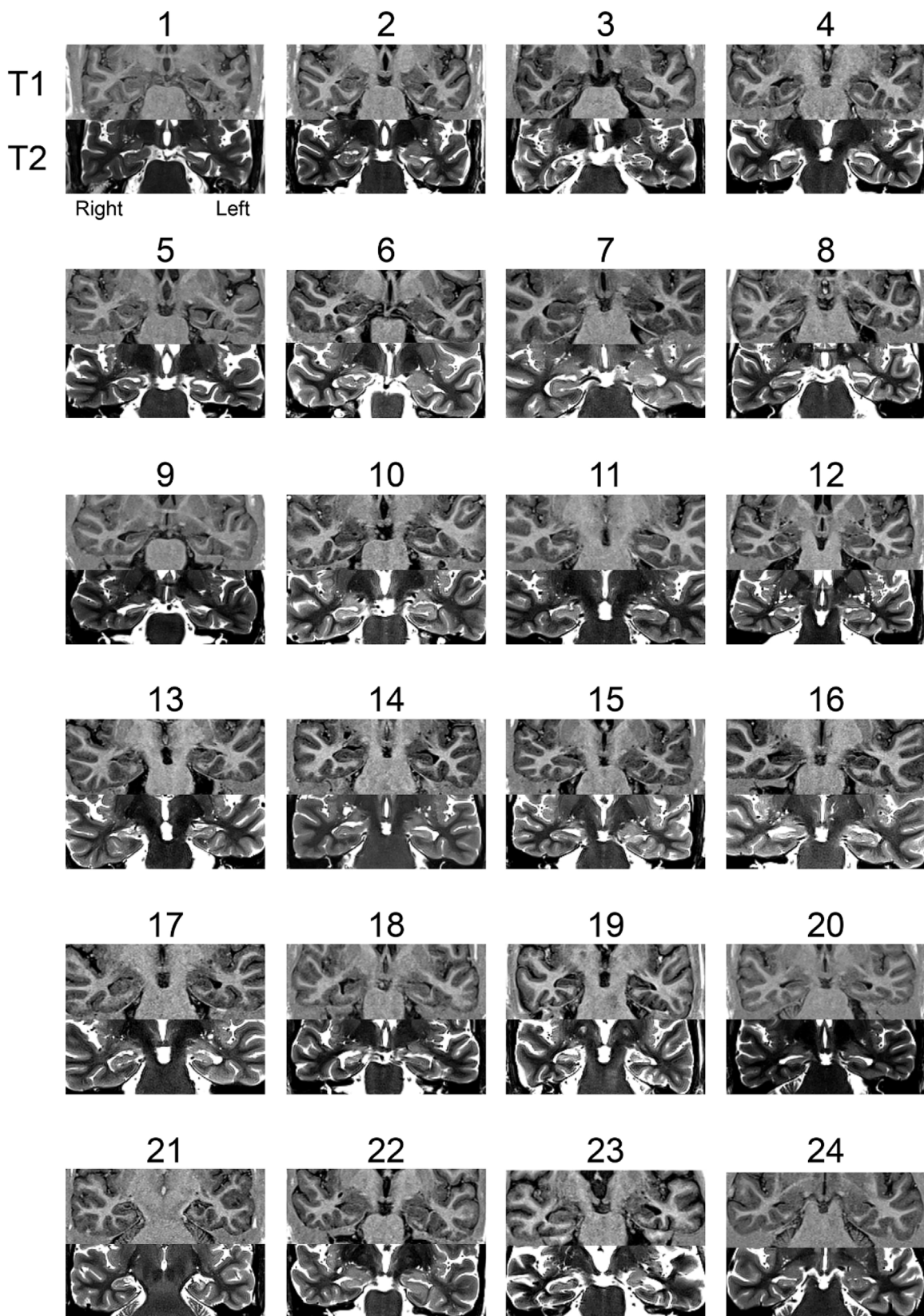


**Fig. 1.** Magnetic resonance imaging findings of 24 patients with mesial temporal lobe epilepsy. Numbers indicate the patients (see Table 1 for more clinical and EEG details). For each individual, coronal slices in T1 (superior row) and T2 (inferior row) sequences are demonstrated. Images are in radiological orientation with the slice including the anterior portion of the hippocampus.

**Table 2**

Results of voxel-based analysis comparing axial diffusivity (AD), radial diffusivity (RD), mean diffusivity (MD), and fractional anisotropy (FA) maps of 24 patients with medial temporal lobe epilepsy to those of 36 controls according to two methodologies: whole brain voxel-wise analysis and tract-based spatial statistics.

Method	Parameter	Volume (mm <sup>3</sup> )	P-value	Coordinates	Localization	
					Talairach	JHU
Whole brain voxel-wise analysis	AD	290	0.001	31, -18, -24	Parahippocampal	Right cingulum (hippocampus)
		758	<0.0001	28, -16, -25	Parahippocampal	Right cingulum (hippocampus)
		344	<0.0001	-34, -10, -15	Temporal lobe	Left inferior fronto-occipital, uncinate, inferior longitudinal
	MD	595	<0.0001	29, -17, -24	Parahippocampal	Right cingulum (hippocampus)
		187	0.003	-32, -10, -15	Parahippocampal	Left inferior longitudinal, anterior thalamic radiation
	FA	719	<0.0001	-33, -11, -13	Sub-lobar	Left uncinate, inferior fronto-occipital
		624	<0.0001	34, -3, -15	Temporal lobe	Right inferior fronto-occipital, anterior thalamic radiation, inferior longitudinal
	RD	234	0.001	-40, -33, -3	Temporal lobe	Left inferior fronto-occipital, inferior longitudinal, superior longitudinal
		57	0.011	-22, -6, 32	Sub-lobar	Left inferior longitudinal, anterior thalamic radiation
	Tract-based spatial statistics	51	0.012	-26, -28, -2	Frontal lobe	Left superior longitudinal
		423	0.028	-39, 7, -30	Superior temporal	Left inferior longitudinal, uncinate, inferior fronto-occipital
		1132	0.001	-38, -10, -19	Temporal lobe	Left anterior thalamic radiation, inferior longitudinal, inferior fronto-occipital
Tract-based spatial statistics	MD	412	0.001	28, 4, -35	Uncus	Right inferior longitudinal
		254	0.008	28, 4, -35	Uncus	Right inferior longitudinal
		69	0.009	-42, -7, -22	Temporal lobe	Left inferior longitudinal, uncinate, superior longitudinal, inferior fronto-occipital
	FA	17581	<0.001	-39, -5, -36	Temporal lobe	Left inferior longitudinal
		1332	<0.001	42, -3, -35	Middle temporal	Right inferior longitudinal
		523	0.001	39, -40, 18	Superior temporal	Right superior longitudinal
		205	0.001	32, -49, 18	Temporal lobe	Right inferior fronto-occipital, inferior longitudinal, superior longitudinal, forceps major

Results correspond to areas of increased AD, RD, MD and reduced FA. Coordinates are in Montreal Neurological Institute space (MNI; x, y, z). Localization was identified according to the Talairach atlas and the Johns Hopkins University white-matter tractography atlas (Talairach and Tournoux, 1988; Mori, 2005).

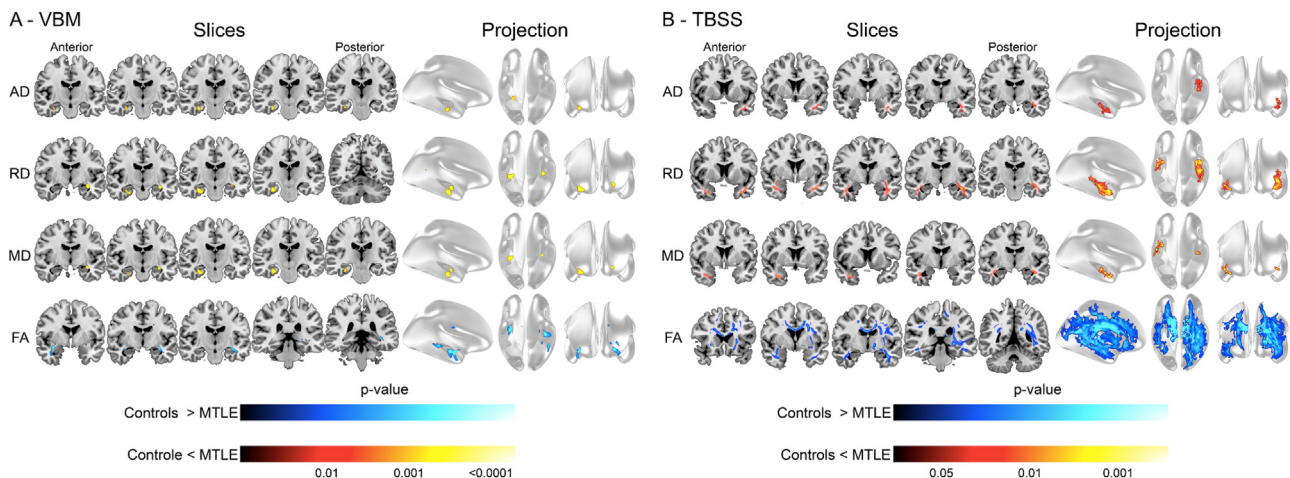


**Fig. 2.** Results of the voxel-based analysis comparing the maps of axial diffusivity (AD), radial diffusivity (RD), mean diffusivity (MD) and fractional anisotropy (FA) of 24 patients with medial temporal lobe epilepsy to 36 controls. Two methodologies were used (whole brain voxel-wise analysis and tract-based spatial statistics). The results (colored areas) are codified according to the p-value (depicted in the color scale at the bottom of the figure) and overlaid in coronal slices of an anatomical template of the brain (Slices). A tridimensional inflated brain model also shows the projection of all abnormal areas. Orientation is radiological.

cili ( $x = -33, y = -11, z = -13$ ;  $T$  value = 6.44;  $Z$  = 5.54;  $p < 0.0001$ ). Table 2 and Fig. 2 show these findings. Areas of reduced AD, RD, MD and increased FA were not disclosed.

For patients with right MTLE, we obtained: two clusters of increased AD, volume of 203 mm<sup>3</sup>, main localization in the right hippocampus and parahippocampal gyrus ( $x = 30, y = -17, z = -24$ ;  $T$  value = 5.9;  $Z$  = 5.16;  $p = 0.003$ ); two clusters of increased RD, total volume of 360 mm<sup>3</sup>, main localization in the right hip-

pocampus and parahippocampal gyrus ( $x = 26, y = -17, z = -25$ ;  $T$  value = 6.36;  $Z$  = 5.47;  $p = 0.001$ ); three clusters of increased MD, total volume of 338 mm<sup>3</sup>, main localization in the right hippocampus and parahippocampal gyrus ( $x = 27, y = -17, z = -25$ ;  $T$  value = 6.30;  $Z$  = 5.43;  $p = 0.001$ ); two clusters of reduced FA, total volume of 371 mm<sup>3</sup>, main localization in the right temporal lobe involving the uncinate, inferior fronto-occipital and inferior longitudinal fasciculi ( $x = -33, y = -1, z = -13$ ;  $T$  value = 6.81;  $Z$  = 5.76;  $p$

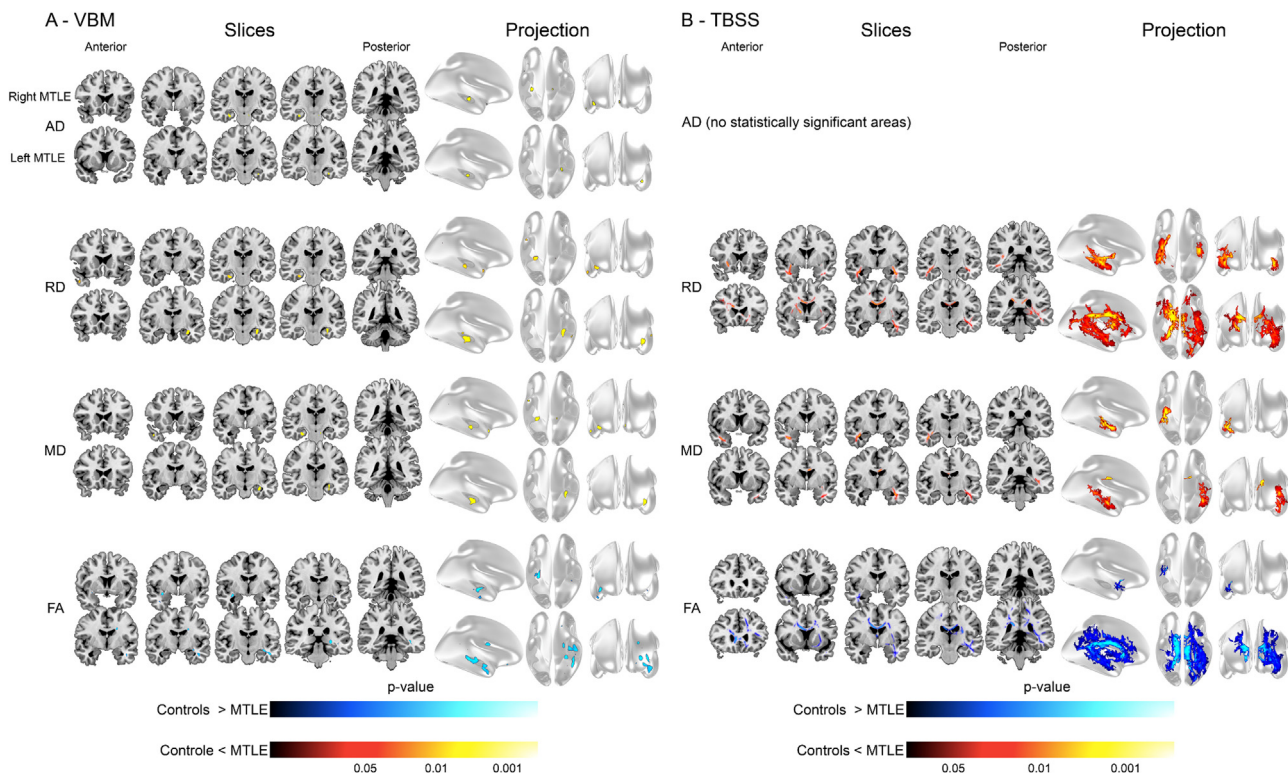


**Fig. 3.** Results of the voxel-based analysis comparing the maps of axial diffusivity (AD), radial diffusivity (RD), mean diffusivity (MD) and fractional anisotropy (FA) of 10 patients with right (superior rows) and 14 with left (inferior rows) medial temporal lobe epilepsy to 36 controls. Two methodologies were used (whole brain voxel-wise analysis and tract-based spatial statistics). The results (colored areas) are codified according to the *p*-value (depicted in the color scale at the bottom of the figure) and overlaid in coronal slices of an anatomical template of the brain (Slices). A tridimensional inflated brain model also shows the projection of all abnormal areas. Orientation is radiological.

<0.0001). Fig. 3 show these findings. Areas of reduced AD, RD, MD and increased FA were not disclosed.

For patients with left MTLE, we obtained: one cluster of increased AD, volume of  $81 \text{ mm}^3$ , main localization in the left hippocampus and parahippocampal gyrus ( $x = -29, y = -17, z = -23$ ;  $T$  value = 5.66;  $Z = 5$ ;  $p = 0.009$ ); two clusters of increased RD, total volume of  $735 \text{ mm}^3$ , main localization in the left parahippocampal gyrus involving the anterior thalamic radiation ( $x = -32, y = -12, z = -18$ ;  $T$  value = 6.50;  $Z = 5.56$ ;  $p < 0.0001$ ); one cluster of increased MD, total volume of  $456 \text{ mm}^3$ , main localization in the left parahippocampal gyrus involving the inferior longitudinal fasciculus ( $x = -30, y = -12, z = -18$ ;  $T$  value = 6.17;  $Z = 5.34$ ;  $p = 0.005$ ); four clusters of reduced FA, total volume of  $1505 \text{ mm}^3$ , main localization in the left parahippocampal gyrus involving the inferior longitudinal fasciculi ( $x = -27, y = -28, z = 0$ ;  $T$  value = 5.82;  $Z = 5.11$ ;  $p = 0.001$ ). Fig. 3 show these findings. Areas of reduced AD, RD, MD and increased FA were not disclosed.

#### 3.4. TBSS analysis

For the whole group of patients, it was obtained: one cluster of increased AD, volume of  $423 \text{ mm}^3$ , localization in the left superior temporal gyrus involving the inferior longitudinal, uncinate and inferior fronto-occipital fasciculi ( $x = -39, y = 7, z = -30$ ;  $p = 0.028$ ); two clusters of increased RD, total volume of  $1544 \text{ mm}^3$ , main localization in the left temporal lobe involving the anterior thalamic radiation, inferior longitudinal and inferior fronto-occipital fasciculi ( $x = -38, y = -10, z = -19$ ;  $p = 0.001$ ); two clusters of increased MD, total volume of  $323 \text{ mm}^3$ , main localization in the right uncus involving the inferior longitudinal fasciculus ( $x = 28, y = 4, z = -35$ ;  $p = 0.008$ ); four clusters of reduced FA, total volume of  $19641 \text{ mm}^3$ , main localization in the left temporal lobe involving the inferior

longitudinal fasciculus ( $x = -39, y = -5, z = -36$ ;  $p < 0.001$ ). Table 2 and Fig. 2 show these findings. Areas of reduced AD, RD, MD and increased FA were not disclosed.

For patients with right MTLE, it was obtained: two clusters of increased RD, volume of  $2663 \text{ mm}^3$ , main localization in the right temporal lobe involving the inferior longitudinal fasciculus ( $x = 42, y = -3, z = -27$ ;  $p = 0.008$ ); one cluster of increased MD, total volume of  $675 \text{ mm}^3$ , main localization in the right temporal lobe involving the inferior longitudinal fasciculus ( $x = 31, y = 8, z = -34$ ;  $p = 0.023$ ); one cluster of reduced FA, total volume of  $514 \text{ mm}^3$ , main localization in the right middle temporal gyrus involving the inferior longitudinal fasciculus ( $x = 42, y = -3, z = -35$ ;  $p = 0.005$ ). Fig. 3 shows these findings. Areas of reduced AD, RD, MD and increased AD and FA were not disclosed.

For patients with left MTLE, it was obtained: four clusters of increased RD, volume of  $8478 \text{ mm}^3$ , main localization in the left superior temporal lobe involving the inferior longitudinal fasciculus and anterior thalamic radiation ( $x = -34, y = 4, z = -31$ ;  $p = 0.001$ ); three clusters of increased MD, total volume of  $1643 \text{ mm}^3$ , main localization in the left temporal lobe involving mainly the inferior longitudinal fasciculus ( $x = -42, y = -7, z = -22$ ;  $p = 0.011$ ); one cluster of reduced FA, total volume of  $17928 \text{ mm}^3$ , main localization in the left temporal lobe involving the inferior longitudinal fasciculus ( $x = -39, y = -5, z = -36$ ;  $p < 0.001$ ). Fig. 3 shows these findings. Areas of reduced AD, RD, MD and increased AD and FA were not disclosed.

#### 3.5. TSA analysis

TSA showed increased AD, RD and MD as well as reduced FA in patients with MTLE. For the whole group analysis, RD ( $5442 \text{ mm}^2$ ) and MD ( $5496 \text{ mm}^2$ ) were the parameters with the larger affected

**Table 3**

Results of tract-specific analysis comparing axial diffusivity (AD), radial diffusivity (RD), mean diffusivity (MD) and fractional anisotropy (FA) maps of 24 patients with medial temporal lobe epilepsy to those of 36 controls.

Parameter	Area (mm <sup>2</sup> )	P-value	T value (mean)	Hemisphere	Localization
AD	645	0.002	2.49	left	Inferior fronto-occipital
	316	0.002	2.88	left	Uncinate
	319	0.0012	2.58	right	Uncinate
RD	217	0.044	1.87	left	Inferior longitudinal
	813	0.003	2.17	right	Inferior longitudinal
	425	0.02	1.98	right	Inferior longitudinal
	1108	0.001	2.87	left	Inferior fronto-occipital
	637	0.008	1.87	left	Inferior fronto-occipital
	797	0.007	2.98	right	Inferior fronto-occipital
	419	0.007	2.08	left	Superior longitudinal
	300	0.024	1.81	left	Superior longitudinal
	301	0.005	2.45	left	Uncinate
	425	<0.0001	3.03	right	Uncinate
MD	949	0.005	2.18	right	Inferior longitudinal
	369	0.043	2.03	right	Inferior longitudinal
	1006	0.002	2.96	left	Inferior fronto-occipital
	781	0.004	2.1	left	Inferior fronto-occipital
	1132	0.007	2.89	right	Inferior fronto-occipital
	496	0.003	1.89	left	Superior longitudinal
	322	0.003	2.67	left	Uncinate
FA	441	<0.0001	2.98	right	Uncinate
	291	0.032	1.83	right	Inferior longitudinal
	864	0.0006	2.41	left	Inferior fronto-occipital
	244	0.04	2.54	right	Inferior fronto-occipital
	259	0.022	2.13	left	Superior longitudinal
	180	0.017	2.77	right	Uncinate

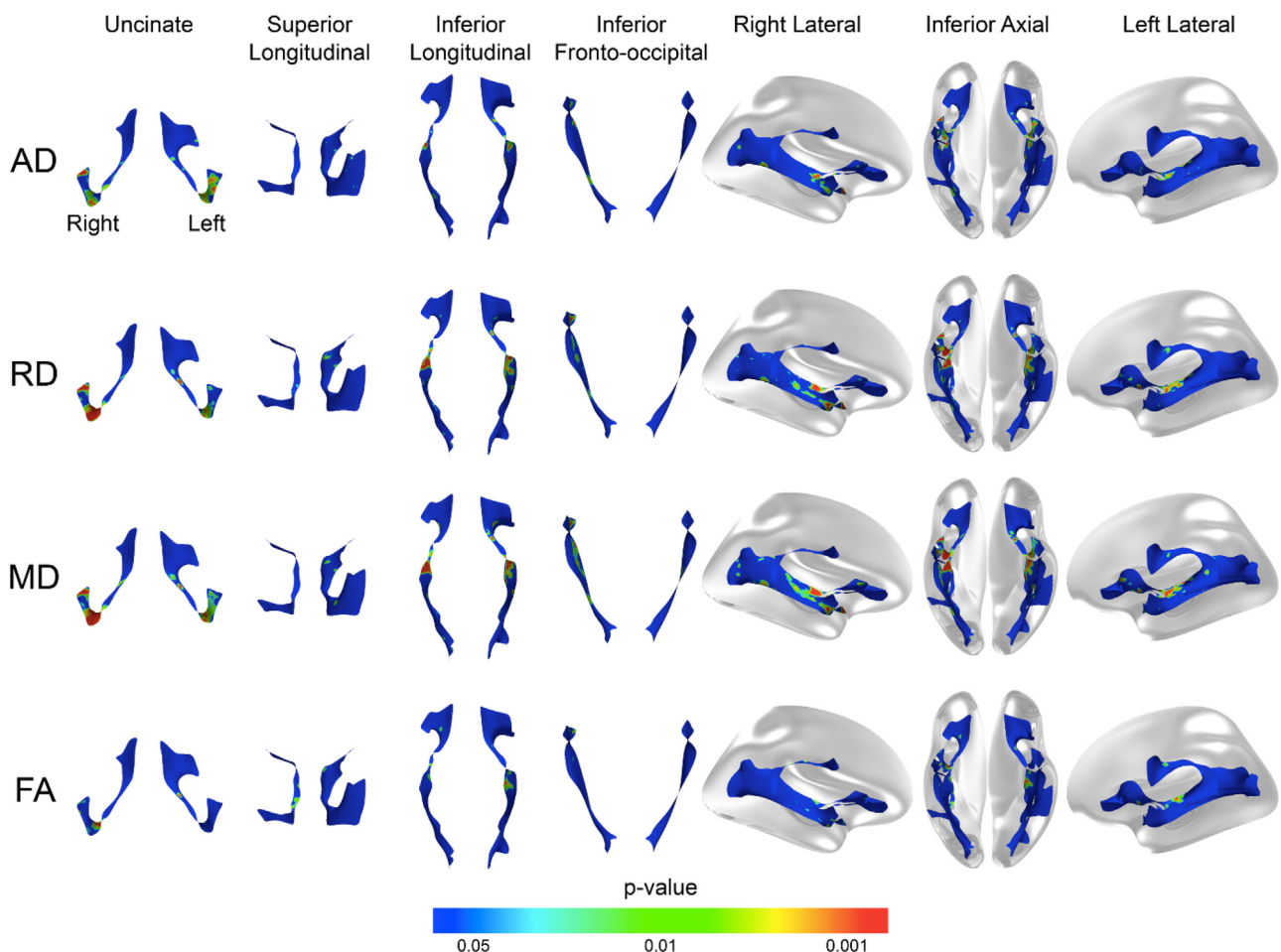


**Fig. 4.** Results of the tract-specific analysis comparing the maps of axial diffusivity (AD), radial diffusivity (RD), mean diffusivity (MD) and fractional anisotropy (FA) of 24 patients with medial temporal lobe epilepsy to 36 controls. Results (colored areas) are codified according to the p-value (depicted in the color scale at the bottom of the figure) and overlaid in the flattened tridimensional model of the fasciculi. An overlay of all fasciculi with a tridimensional inflated brain model is also depicted.

areas, followed by FA ( $1838 \text{ mm}^2$ ) and AD ( $1280 \text{ mm}^2$ ). The distribution of the abnormalities was mainly in inferior fronto-occipital ( $7214 \text{ mm}^2$ ) and inferior longitudinal ( $3064 \text{ mm}^2$ ) regions followed by the uncinate ( $2304 \text{ mm}^2$ ) and superior longitudinal fasciculi ( $1474 \text{ mm}^2$ ). There were no areas of reduced AD, RD or MD, nor of increased FA. Table 3 and Fig. 4 show these findings in detail.

For patients with right MTLE, RD ( $3167 \text{ mm}^2$ ) and MD ( $2812 \text{ mm}^2$ ) were the parameters with the larger affected areas, followed by FA ( $1878 \text{ mm}^2$ ) and AD ( $272 \text{ mm}^2$ ). RD, MD and FA showed bilateral areas of abnormalities. The distribution of the abnormalities was mainly in inferior fronto-occipital ( $3045 \text{ mm}^2$ ) and inferior longitudinal ( $3010 \text{ mm}^2$ ) followed by the uncinate fasciculi ( $2347 \text{ mm}^2$ ). Inferior fronto-occipital and inferior longitudinal fasciculi showed bilateral areas of abnormalities. There were no areas of reduced AD, RD or MD, nor of increased FA.

For patients with left MTLE, RD ( $4527 \text{ mm}^2$ ) and MD ( $3578 \text{ mm}^2$ ) were the parameters with the larger affected areas, followed by AD ( $1356 \text{ mm}^2$ ) and FA ( $1298 \text{ mm}^2$ ). AD, RD and MD showed bilateral areas of abnormalities. The distribution of the abnormalities was mainly in inferior fronto-occipital ( $4982 \text{ mm}^2$ ) and superior longitudinal ( $2032 \text{ mm}^2$ ) followed by the uncinate ( $1883 \text{ mm}^2$ ) and inferior longitudinal fasciculi ( $1862 \text{ mm}^2$ ). Inferior fronto-occipital, inferior longitudinal and uncinate fasciculi showed bilateral areas of abnormalities. There were no areas of reduced AD, RD or MD, nor of increased FA.

#### 4. Discussion

In this investigation different patterns of diffusion abnormalities were observed in patients with MTLE depending on the methodology and the diffusion parameter used. For the voxel-based analysis investigation, FA and RD were the parameters that showed more abnormalities. Therefore, they should be routinely used in the quantitative investigation of diffusion abnormalities in MTLE.

Clinical interpretation of DTI parameters is complex and should be performed with care (Alexander et al., 2007). To maximize the specificity of the DTI investigation, the use of several parameters, such as FA, AD, and RD, is recommended. FA is reduced in several conditions and is considered a marker of fiber integrity but this is an over-simplification. FA basically indicates that orientation dependent aspects of the brain microstructure are different (Jones et al., 2013). Decreasing axonal density, increasing axonal caliber and reducing the degree of myelination should all lead to increased RD and reduced FA (Jones et al., 2013). AD indicates the main fiber orientation. Most investigations of patients with MTLE have used FA and MD. In this study, AD was the parameter with the fewest abnormalities, followed by MD, RD and FA respectively. Considering the limitations, these findings may be related with an active inflammatory process and are in line with pathological investigations of surgical patients (Crespel et al., 2002).

The present whole brain voxel-wise and TBSS results indicated the presence of abnormalities in 80% of cases in the superior and inferior longitudinal, inferior fronto-occipital and uncinate fasciculi. These white matter fasciculi have a diffuse intra hemispheric localization extending in the axial orientation of the brain. Our findings demonstrate a massive involvement of the temporal lobe white matter with abnormalities in the intricate network of fasciculi that run through this region. The TSA results further revealed major abnormalities in temporal stem topography encompassing the inferior fronto-occipital, inferior longitudinal and uncinate fasciculi in 90% of cases. Prior research investigating white matter connectivity in MTLE patients has suggested that differences in resections of this circuitry may contribute to different surgical outcomes (Bonilha et al., 2013).

There are investigations suggesting that patients with HS have more widespread abnormalities than patients with a normal MRI (Scanlon et al., 2013). Indeed, patients with left HS are also predisposed to having more diffuse abnormalities (Ahmadi et al., 2009). However, these findings are not uniform (Rodriguez-Cruces and Concha, 2015). The patients investigated here were heterogeneous. Patients had mainly unilateral HS, but bilateral patients were also included. In our study, comparisons according to HS side revealed broad abnormalities in left MTLE.

In patients with MTLE, white matter abnormalities have been localized to the temporal and extra-temporal regions with a centrifugal pattern (Gross, 2011; Otte et al., 2012). Astrogliosis and microstructure rearrangement near the focus and postictal vasogenic edema distally may be related to this pattern (Concha et al., 2012). White matter abnormalities may be observed in up to 63% of patients submitted to surgical treatment (Kasper et al., 1999; Rodriguez-Cruces and Concha, 2015). The main histological abnormalities described are axonal and myelinic abnormalities, heterotopic neurons in the white matter, blurring of the gray-white matter boundary and white matter gliosis. Reduced axonal density is consistently reported, and the increased extra-cellular space explains the increment of MD and reduction of FA observed in previous investigations (Rodriguez-Cruces and Concha, 2015).

It remains unclear which methodology of voxel-based analysis is the best to evaluate patients with MTLE. Two investigations compared voxel-based analysis using SPM versus TBSS. In one study in which FA and MD of 33 patients with MTLE were investigated, Focke et al. (2008) found widespread abnormalities in the temporal lobe mainly ipsilateral to the HS. Similar to the present study, they found that TBSS was more sensitive to changes for white matter abnormalities. Subsequently, in a study examining FA and ellipsoidal area ratio in 19 patients with MTLE, Afzali et al. (2011) found that TBSS abnormalities were most prominent in the temporal lobe and parahippocampal gyrus. Meanwhile, SPM analysis disclosed abnormalities mainly in the temporal lobes, corpus callosum and fornix. The authors concluded that TBSS was relatively more localized and that ellipsoidal area ratio was more sensitive to white matter abnormalities than FA. Both investigations used conventional registration of the images.

Registration is a critical issue in voxel-based analysis. Without careful performance and checking of this procedure, false positive results may occur (Bookstein, 2001; Schwarz et al., 2014). In this study, registration was performed with the use of the tensor map as is recommended for DTI (Wang et al., 2011). This approach uses full tensor information to drive a more precise alignment (Keihaninejad et al., 2013).

The restriction of our whole brain voxel-wise analysis results to the temporal lobe may be related to the use of Family-Wise Error correction in the statistical analysis. It has been suggested that this threshold may be too rigorous and omit true positive results (Henley et al., 2010). Although a similar correction was applied in our TBSS, the different statistical approach used for the TBSS likely minimized this effect (Winkler et al., 2014), yielding the identification of more regionally extensive abnormalities, especially for FA. These findings are in agreement with the notion that MTLE patients suffer from extra-temporal abnormalities.

One drawback of this investigation was the number of diffusion directions acquired. A large number of sampling orientations is recommended to avoid biases (Jones, 2004). However, for this investigation, this impact was reduced because the main objective was not to develop detailed representation of structural abnormalities. This study was designed to access variation across the main diffusion parameters and to compare two techniques of voxel-based analysis when applied to DTI images acquired using the same protocol.

## 5. Conclusion

The findings here lend support that different approaches may contribute to the current knowledge of the mechanisms behind MTLE. The use of all diffusion parameters and distinct techniques is advised because they may show additional findings.

## Conflicts of interest

None.

## Acknowledgement

Supported by grants number 2011/02961-2 and 2016/17914-3, São Paulo Research Foundation (FAPESP).

## References

- Abe, O., Takao, H., Gotoi, W., et al., 2010. Voxel-based analysis of the diffusion tensor. *Neuroradiology* 52, 699–710.
- Afzali, M., Soltanian-Zadeh, H., Elisevich, K.V., 2011. Tract based spatial statistical analysis and voxel based morphometry of diffusion indices in temporal lobe epilepsy. *Comput. Biol. Med.* 41, 1082–1091.
- Ahmadi, M.E., Hagler Jr., D.J., McDonald, C.R., et al., 2009. Side matters: diffusion tensor imaging tractography in left and right temporal lobe epilepsy. *AJNR Am. J. Neuroradiol.* 30, 1740–1747.
- Alexander, A.L., Lee, J.E., Lazar, M., Field, A.S., 2007. Diffusion tensor imaging of the brain. *Neurotherapeutics* 4, 316–329.
- Ashburner, J., Friston, K.J., 2000. Voxel-based morphometry—the methods. *Neuroimage* 11, 805–821.
- Bach, M., Laun, F.B., Leemans, A., et al., 2014. Methodological considerations on tract-based spatial statistics (TBSS). *Neuroimage* 100, 358–369.
- Behrens, T.E., Woolrich, M.W., Jenkinson, M., et al., 2003. Characterization and propagation of uncertainty in diffusion-weighted MR imaging. *Magn. Reson. Med.* 50, 1077–1088.
- Berg, A.T., Berkovic, S.F., Brodie, M.J., et al., 2010. Revised terminology and concepts for organization of seizures and epilepsies: report of the ILAE Commission on Classification and Terminology, 2005–2009. *Epilepsia* 51, 676–685.
- Bonilha, L., Helpern, J.A., Sainju, R., et al., 2013. Presurgical connectome and postsurgical seizure control in temporal lobe epilepsy. *Neurology* 81, 1704–1710.
- Bookstein, F.L., 2001. Voxel-based morphometry should not be used with imperfectly registered images. *Neuroimage* 14, 1454–1462.
- Commission on Classification and Terminology of the International League Against Epilepsy, 1989. Proposal for revised classification of epilepsies and epileptic syndromes. *Epilepsia* 30, 389–399.
- Concha, L., Kim, H., Bernasconi, A., Bernhardt, B.C., Bernasconi, N., 2012. Spatial patterns of water diffusion along white matter tracts in temporal lobe epilepsy. *Neurology* 79, 455–462.
- Crespel, A., Coubes, P., Rousset, M.C., et al., 2002. Inflammatory reactions in human medial temporal lobe epilepsy with hippocampal sclerosis. *Brain Res.* 952, 159–169.
- Fischl, B., Salat, D.H., Busa, E., et al., 2002. Whole brain segmentation: automated labeling of neuroanatomical structures in the human brain. *Neuron* 33, 341–355.
- Fischl, B., van der Kouwe, A., Destrieux, C., et al., 2004. Automatically parcellating the human cerebral cortex. *Cereb. Cortex* 14, 11–22.
- Focke, N.K., Yogarajah, M., Bonelli, S.B., et al., 2008. Voxel-based diffusion tensor imaging in patients with mesial temporal lobe epilepsy and hippocampal sclerosis. *Neuroimage* 40, 728–737.
- Gross, D.W., 2011. Diffusion tensor imaging in temporal lobe epilepsy. *Epilepsia* 52 (Suppl. 4), 32–34.
- Henley, S.M., Ridgway, G.R., Scahill, R.I., et al., 2010. Pitfalls in the use of voxel-based morphometry as a biomarker: examples from huntington disease. *AJR Am. J. Neuroradiol.* 31, 711–719.
- Jenkinson, M., Beckmann, C.F., Behrens, T.E., Woolrich, M.W., Smith, S.M., 2012. Fsl. *Neuroimage* 62, 782–790.
- Jones, D.K., Knösche, T.R., Turner, R., 2013. White matter integrity, fiber count, and other fallacies: the do's and don'ts of diffusion MRI. *Neuroimage* 73, 239–254.
- Jones, D.K., 2004. The effect of gradient sampling schemes on measures derived from diffusion tensor MRI: a Monte Carlo study. *Magn. Reson. Med.* 51, 807–815.
- Kasper, B.S., Stefan, H., Buchfelder, M., Paulus, W., 1999. Temporal lobe microdysgenesis in epilepsy versus control brains. *J. Neuropathol. Exp. Neurol.* 58, 22–28.
- Keihaninejad, S., Zhang, H., Ryan, N.S., et al., 2013. An unbiased longitudinal analysis framework for tracking white matter changes using diffusion tensor imaging with application to Alzheimer's disease. *Neuroimage* 72, 153–163.
- Mori, S., 2005. *MRI Atlas of Human White Matter*, 1st ed. Elsevier, Amsterdam; Boston.
- Otte, W.M., van Eijnsden, P., Sander, J.W., Duncan, J.S., Dijkhuizen, R.M., Braun, K.P., 2012. A metaanalysis of white matter changes in temporal lobe epilepsy as studied with diffusion tensor imaging. *Epilepsia* 53, 659–667.
- Rodriguez-Cruces, R., Concha, L., 2015. White matter in temporal lobe epilepsy: clinicopathological correlates of water diffusion abnormalities. *Quant. Imaging Med. Surg.* 5, 264–278.
- Rorden, C., Brett, M., 2000. Stereotaxic display of brain lesions. *Behav. Neurol.* 12, 191–200.
- Scanlon, C., Mueller, S.G., Cheong, I., Hartig, M., Weiner, M.W., Laxer, K.D., 2013. Grey and white matter abnormalities in temporal lobe epilepsy with and without mesial temporal sclerosis. *J. Neurol.* 260, 2320–2329.
- Schwarz, C.G., Reid, R.I., Gunter, J.L., et al., 2014. Improved DTI registration allows voxel-based analysis that outperforms tract-based spatial statistics. *Neuroimage* 94, 65–78.
- Smith, S.M., Jenkinson, M., Johansen-Berg, H., et al., 2006. Tract-based spatial statistics: voxelwise analysis of multi-subject diffusion data. *Neuroimage* 31, 1487–1505.
- Smith, S.M., 2002. Fast robust automated brain extraction. *Hum. Brain Mapp.* 17, 143–155.
- Talairach, J., Tournoux, P., 1988. *Co-planar Stereotaxic Atlas of the Human Brain : 3-dimensional Proportional System: an Approach to Cerebral Imaging*. Thieme Medical Publishers, Stuttgart; New York; G. Thieme; New York.
- Wang, Y., Gupta, A., Liu, Z., et al., 2011. DTI registration in atlas based fiber analysis of infantile Krabbe disease. *Neuroimage* 55, 1577–1586.
- Winkler, A.M., Ridgway, G.R., Webster, M.A., Smith, S.M., Nichols, T.E., 2014. Permutation inference for the general linear model. *Neuroimage* 92, 381–397.
- Yasuda, C.L., Betting, L.E., Cendes, F., 2010. Voxel-based morphometry and epilepsy. *Expert Rev. Neurother.* 10, 975–984.
- Yushkevich, P.A., Zhang, H., Simon, T.J., Gee, J.C., 2008. Structure-specific statistical mapping of white matter tracts. *Neuroimage* 41, 448–461.
- Zhang, H., Yushkevich, P., Rueckert, D., Gee, J., 2010. A computational white matter atlas for aging with surface-based representation of fasciculi. In: Fischer, B., Dawant, B., Lorenz, C. (Eds.), *Biomedical Image Registration*. Springer, Berlin Heidelberg, pp. 83–90.
- Zhang, S., Peng, H., Dawe, R.J., Arfanakis, K., 2011. Enhanced ICBM diffusion tensor template of the human brain. *Neuroimage* 54, 974–984.